Cell Death and Differentiation (2014) 21, 1733–1745

www.nature.com/cdd

Mitochondrial Ca^{2+} influx targets cardiolipin to disintegrate respiratory chain complex II for cell death induction

M-S Hwang[1], CT Schwall[2], E Pazarentzos[1], C Datler[1], NN Alder[2] and S Grimm*[,1]

Massive Ca^{2+} influx into mitochondria is critically involved in cell death induction but it is unknown how this activates the organelle for cell destruction. Using multiple approaches including subcellular fractionation, FRET in intact cells, and *in vitro* reconstitutions, we show that mitochondrial Ca^{2+} influx prompts complex II of the respiratory chain to disintegrate, thereby releasing an enzymatically competent sub-complex that generates excessive reactive oxygen species (ROS) for cell death induction. This Ca^{2+}-dependent dissociation of complex II is also observed in model membrane systems, but not when cardiolipin is replaced with a lipid devoid of Ca^{2+} binding. Cardiolipin is known to associate with complex II and upon Ca^{2+} binding coalesces into separate homotypic clusters. When complex II is deprived of this lipid, it disintegrates for ROS formation and cell death. Our results reveal Ca^{2+} binding to cardiolipin for complex II disintegration as a pivotal step for oxidative stress and cell death induction.
Cell Death and Differentiation (2014) **21,** 1733–1745; doi:10.1038/cdd.2014.84; published online 20 June 2014

Cellular calcium ion (Ca^{2+}) overload is known to be of fundamental importance in pathological cell death induction for instance during brain ischemia, ischemia-reperfusion of the heart, and excitotoxicity of neurons.[1] Upon entering the cytosol from the extracellular space, Ca^{2+} ions accumulate in mitochondria at very high levels. An alternative route into mitochondria, observed during many scenarios of cell death, as well as when therapeutically induced by anticancer agents, is through Ca^{2+} release from the ER. After crossing the ER-mitochondrial junction, the ion is taken up by the mitochondrial calcium uniporter.[2,3] The close apposition of the two organelles ensures that a very high Ca^{2+} concentration can be reached in mitochondria.[4] The direct target of mitochondrial Ca^{2+} influx for cell death induction, however, is unknown.

Cells deficient in complex II of the respiratory chain become resistant to many cell death signals.[5] The ability of this complex to produce deleterious amounts of reactive oxygen species (ROS) has been recognized.[6,7] Initial *in vitro* experiments using blue native gels indicated that during cell death, the sub-complex SDHA/SDHB, which remains enzymatically active,[8] is specifically released from the membrane-anchoring SDHC and SDHD complex II subunits.[9] It can then remove electrons from the substrate succinate and transfer them to molecular oxygen to generate ROS for cell death induction.[5,9]

The principal lipid in the inner mitochondrial membrane that harbors the components of the respiratory chain, including complex II, is the diphosphatidylglycerol cardiolipin. This lipid is known to be involved in cell death, although its effects have been connected mostly with cellular sites different from its most prominent residence.[10–12]

In this study, we investigated whether excessive Ca^{2+} influx into mitochondria can affect on the integrity of complex II and activate this complex for cell death.

Results

Arsenic trioxide (As_2O_3) causes complex II disintegration for ROS production and cell death induction. For detecting the dissociation of complex II, we established a western blot assay based on freeze/thaw and subcellular fractionation to monitor SDHA release into the mitochondrial matrix. As a stimulus for cell death we chose As_2O_3, which is known to induce Ca^{2+} influx into mitochondria[13] as verified by Rhod-2/AM staining (Figure 1a and Supplementary Figure S1a and b). The SDHA protein accumulated in the mitochondrial matrix fraction following 10 h of As_2O_3 treatment before substantial cell death was observed (Figure 1b and Supplementary Figure S1c and d). To monitor the disintegration of complex II in intact cells with a noninvasive method, we engineered a pair of Förster resonance energy transfer (FRET) constructs for SDHB and SDHD fused to enhances yellow fluorescence protein (EYFP) and cyan fluorescence protein (CFP) at the C and the N terminus,

[1]Division of Experimental Medicine, Imperial College London, Hammersmith Campus, Du Cane Road, London W12 0NN, UK and [2]Department of Molecular and Cell Biology, University of Connecticut, 91 N. Eagleville Road, Unit 3125, Storrs, CT 06269-3125, USA
*Corresponding author: S Grimm, Imperial College London, Du Cane Road, London W12 0NN, UK. Tel: +44 20 8383 1593; Fax: +44 20 7594 7393; E-mail: s.grimm@imperial.ac.uk
Abbreviations: FRET, Förster resonance energy transfer; Ca^{2+}, calcium ion; ROS, reactive oxygen species; As_2O_3, arsenic trioxide; EYFP, enhances yellow fluorescence protein; CFP, cyan fluorescence protein; HEK cells, human embryonic kidney cells; PHB, prohibitin; 3-NP, 3-nitropropionic acid; MnSOD, manganese superoxide dismutase; cypD, cyclophilin D; PT-pore, permeability transition pore; POPC, palmitoyloleoylphosphatidylcholine; POPE, palmitoyloleoylphosphatidylethanolamine; CLS1, cardiolipin synthase-1
Received 06.1.14; revised 23.4.14; accepted 15.5.14; Edited by L Scorrano; published online 20.6.14

respectively, which are tightly aligned (Figures 1c and d). Confocal microscopy revealed that the proteins were exclusively localized to mitochondria (Figure 1e). Upon treatment of the cells with 10 μM As_2O_3, we observed a strong reduction in FRET efficiency following an initial drop and recovery (Figure 1f and Supplementary Figure S1e). When we measured the FRET efficiencies before and after 15 h of treatment and included a reference of formaldehyde-fixed cells, HeLa cells displayed a pronounced reduction of the FRET ratios before any sizable cell death was observed (Supplementary Figure S1g and f, right panel). In human embryonic kidney (HEK) cells we detected similar effects

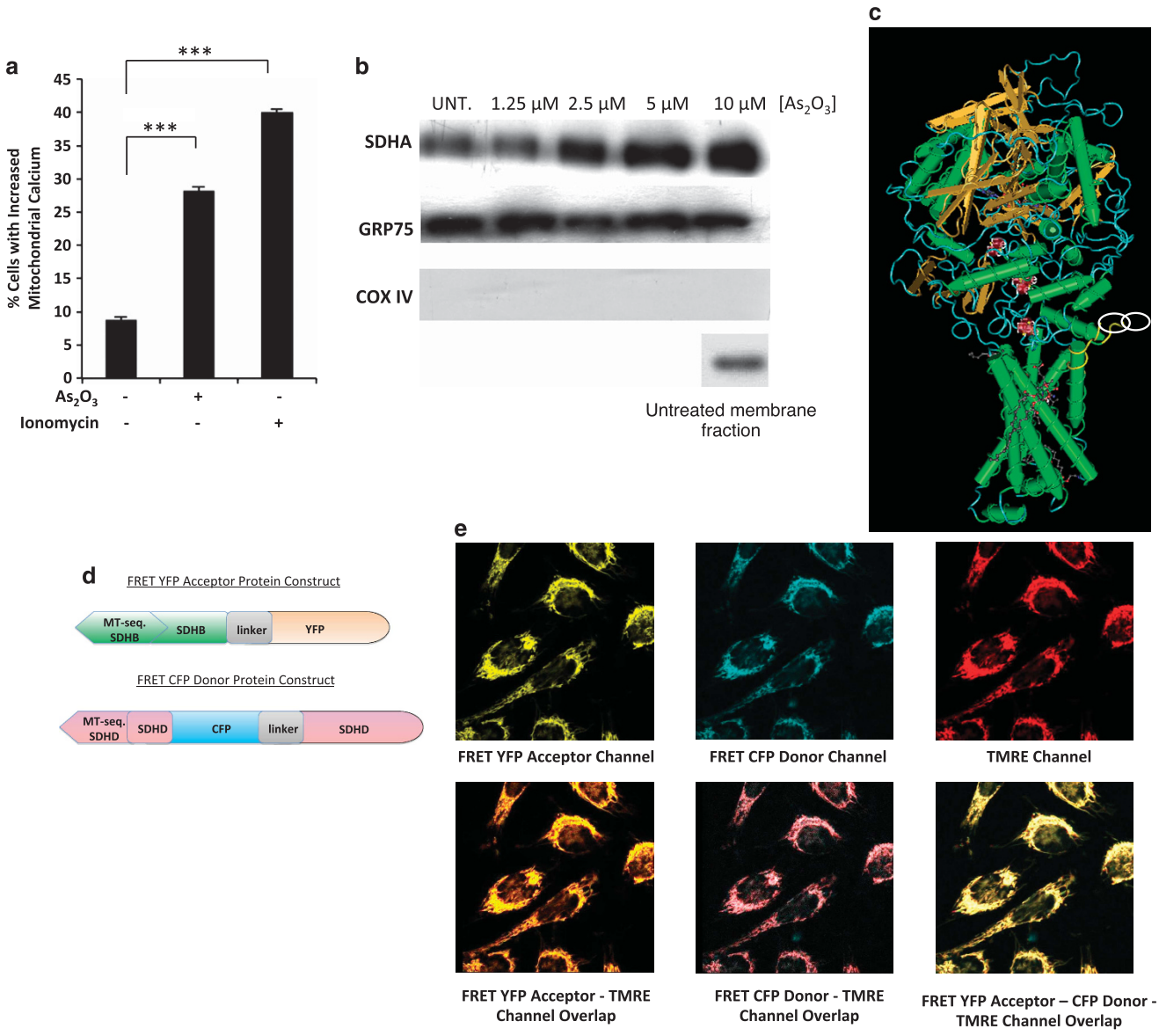

Figure 1 Monitoring complex II disintegration. (**a**) HeLa cells were treated with 10 μM As_2O_3 or with 10 μM ionomycin for 15 h and harvested for Rhod-2-AM staining with FACS analysis to determine the percent cells with increased mitochondrial Ca^{2+}. (**b**) 293T cells were treated with increasing concentrations of As_2O_3 12 h prior to mitochondria isolation and freeze/thaw fractionation. The western blot for the matrix fraction was probed using antibodies against SDHA, GRP75, and COX IV. SDHA is the marker for the dissociation of complex II, GRP75 for the mitochondrial matrix, and COX IV for the mitochondrial inner membrane. A section of the untreated membrane fraction blot of COX IV is shown as an antibody control, taken from the same membrane as the matrix fraction. (**c**) Crystal structure of complex II with location of FRET fusions highlighted. The distance between the N terminus of SDHD (left circle) and the C terminus of SDHB (right circle) is approximately eight Ångströms. Adapted from (Sun, F. 2005). (**d**) The FRET acceptor construct consists of YFP fused to the C terminus of SDHB via a linker sequence. The FRET donor construct comprises CFP fused to the N terminus of SDHD. MT-seq. represents the N-terminal mitochondrial-targeting sequence that is cleaved off upon the protein's import into mitochondria. For the donor construct, a sequence of the mature SDHD sequence was duplicated on the N terminus of CFP, following the MT-seq. to ensure efficient cleavage site recognition. (**e**) Images of HeLa cells taken using a Leica SP5 confocal microscope following transient co-transfection of both FRET YFP acceptor and CPF donor constructs and a TMRE stain to indicate the mitochondria. (**f**) HeLa cells were co-transfected with both FRET constructs, treated as indicated, and monitored over a 13.6-h period. The left plots show signals from the different channels, YFP (green, 514 nm), CFP (red, 458 nm), FRET (blue, resulting from excitation at the donor max and reading at the acceptor), and FRET efficiency (black, right panels) over time in sec x1000. HeLa cells monitored without treatment (top panels), with addition of 1 M NaOH As_2O_3 solvent (middle panels), or with addition of 10 μM As_2O_3 (bottom)

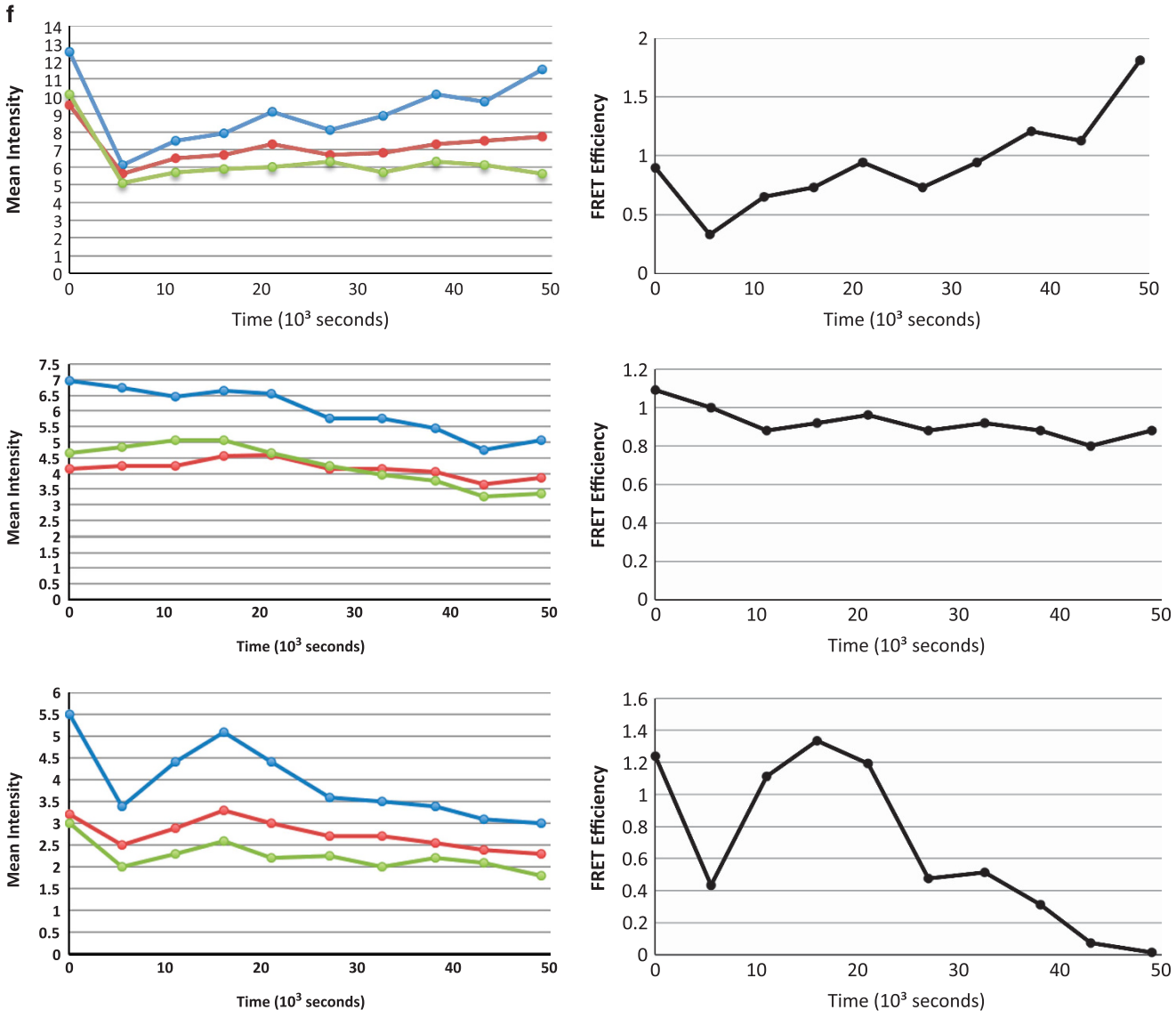

Figure 1 (Continued)

after 10 h (Supplementary Figure S1d and f, left panel). The FRET ratio increased in HeLa cells over time without treatment, an effect that occurred earlier upon transfection (Supplementary Figure S1h).

When an expression plasmid for prohibitin (PHB), the mammalian homolog of the yeast complex II assembly factor Tcm62p,[14] was transfected, the disintegration of the complex by As_2O_3 was efficiently reduced (Figure 2a). No significant change in the subunit levels of complex II subunits was observed upon treatment (Supplementary Figure S1i). In agreement with ROS generation by the released SDHA/SDHB sub-complex, ROS accumulated as measured by the mitochondria-specific dye MitoSOX, which emits a red fluorescent signal upon oxidation by superoxide. This effect was likewise reduced by the expression of PHB (Figure 2b). The dissipation of the mitochondrial membrane potential $\Delta\Psi_m$ as a marker for cell death was likewise diminished by PHB (Figure 2c). As PHB could engage a range of client proteins, we wanted to more specifically target the enzymatic activity of complex II with 3-nitropropionic acid (3-NP), a compound that irreversibly binds to and blocks the catalytic center of SDHA. This inhibitor reduced the amount of ROS generated by As_2O_3 (Figure 2d) but not by menadione (Supplementary Figure S2a) and diminished the extent of cell death (Figure 2e). 3-NP had no effect on the disintegration of complex II (Supplementary Figure S2b). Inhibitors of other complexes of the respiratory chain likewise reduced cell death possibly by stalling the Krebs cycle via NADH, and therefore blocking the supply of the complex II substrate succinate for ROS production (Supplementary Figure S2c). We also observed cell death reduction when we targeted SDHA using RNAi (Supplementary Figure S2d). The importance of ROS formation for cell death caused by As_2O_3 was further emphasized when manganese superoxide dismutase (MnSOD) was

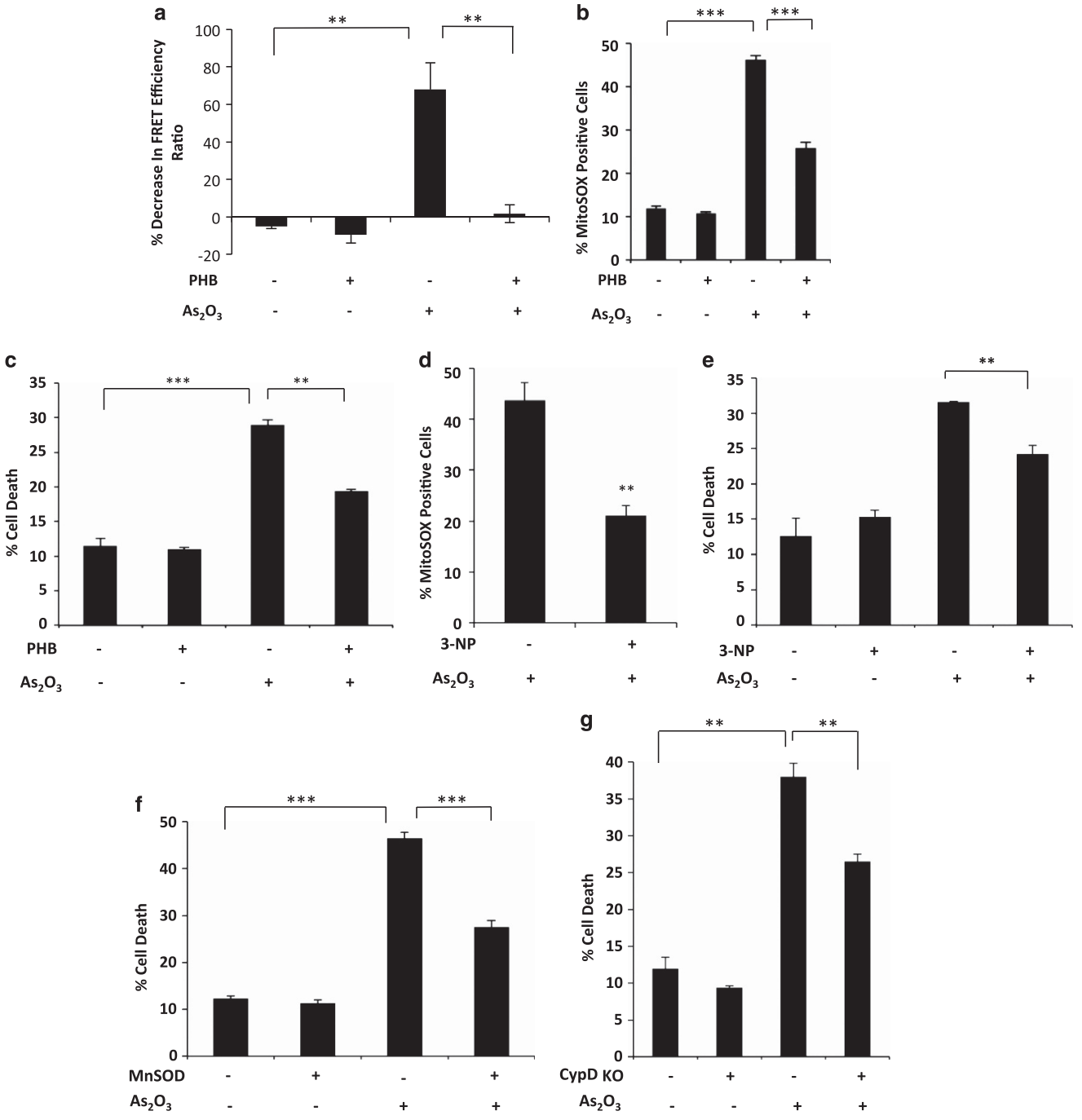

Figure 2 Complex II disintegration by As_2O_3 and the consequences of its reassembly. (**a**) HeLa cells were transfected with pcDNA3 and prohibitin (PHB) 24 h prior to treatment with As_2O_3. Cells were treated with the carrier alone or with 10 μM As_2O_3 for 15 h. FRET efficiency as a measure of complex II dissociation was assessed prior to treatment and 15 h later in triplicates. The two sets of measurements were used to calculate the percent decrease in FRET efficiency ratio with a positive value representing a decrease and a negative value representing an increase. (**b**) HeLa cells were transfected with the empty vector or PHB 24 h prior to treatment with 10 μM As_2O_3 and harvested after 15 h for MitoSOX staining to determine mitochondrial ROS with FACS analysis. (**c**) PHB inhibits cell death upon 10 μM As_2O_3 treatment for 25 h as measured by $DiOC_6$ and PI. (**d**) HeLa cells were treated for 15 h with 10 μM As_2O_3 and then harvested for MitoSOX staining with FACS analysis. 1 mM 3-NP was added to the cells 8 h prior to harvest. The FACS results were used to determine the percent cells with increased ROS generation present within each sample. The MitoSOX-positive cell population in the untreated sample was deducted. (**e**) HeLa cells were treated for 30 h with 10 μM As_2O_3 and harvested for FACS analysis. 1 mM 3-NP was added to the cells 24 h prior to harvest. The FACS results were used to determine the percent cell death present within each sample. (**f**) HeLa cells were transfected with pcDNA3 as a control or MnSOD 24 h prior to treatment with 10 μM As_2O_3 for 25 h and harvested for FACS analysis to determine the percent cell death present within each sample. (**g**) WT and CypD knockout MEF cells were treated for 16 h with 15 μM As2O3 and harvested FACS analysis to determine the percent cell death present within each sample. $^{**}P<0.01$, $^{***}P<0.001$ (student's *t*-test)

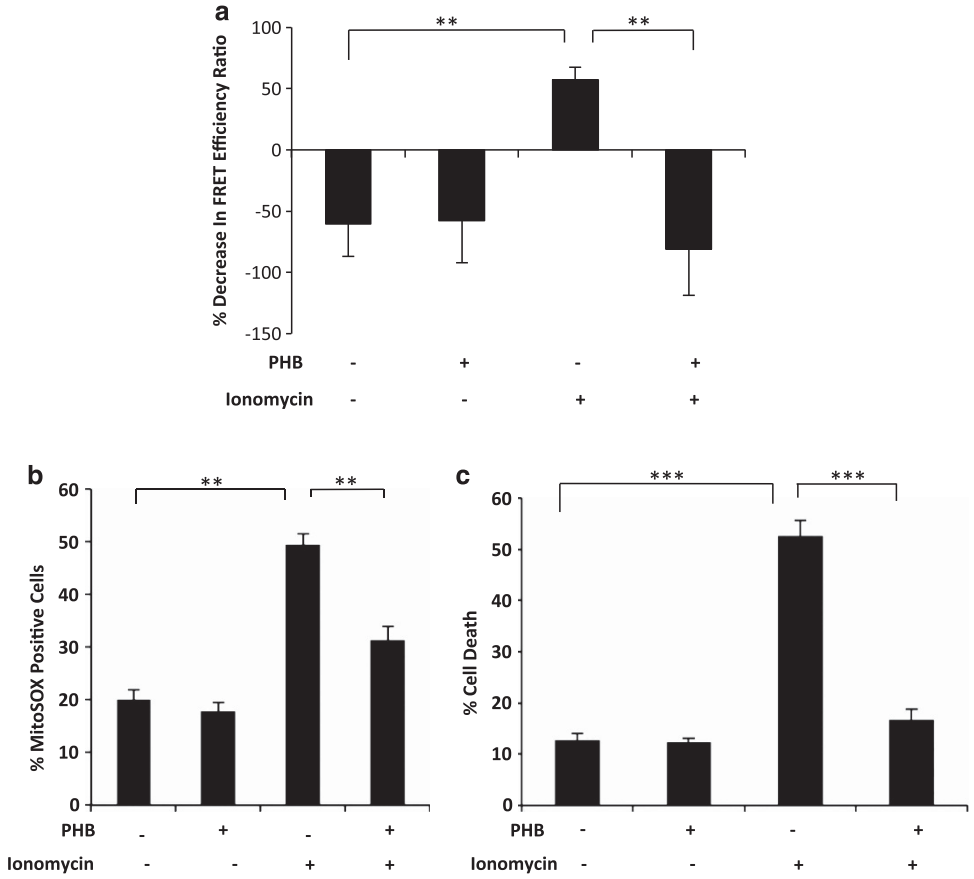

Figure 3 Ca^{2+} influx causes complex II disintegration, ROS formation, and cell death induction. (**a**) HeLa cells were transfected with empty vector or PHB 24 h prior to treatment with 10 μM ionomycin or the carrier DMSO as a control. A calculation for FRET efficiency was made in triplicate for all four sets prior to treatment and four hours post treatment. Data are represented as in Figure 1d. (**b**) HeLa cells were transfected with pcDNA3 as a control or PHB 24 h prior to treatment with 10 μM ionomycin and after eight hours harvested for MitoSOX staining to determine ROS. (**c**) HeLa cells were transfected with pcDNA3 or PHB 24 h prior to treatment for 20 h with 10 μM ionomycin and harvested for $DiOC_6$ and PI stain with FACS analysis. For (**a–c**): $^{**}P<0.01$, $^{***}P<0.001$ (student's *t*-test)

introduced into the cells (Figure 2f). As the permeability transition pore (PT-pore) has been shown to respond to oxidative stress,[15] we wanted to test its involvement. With cyclophilin D (cypD, PPIF) overexpression as well as its knockout, which both inhibit the permeability transition pore (PT-pore) and cell death,[16–20] we probed the involvement of this protein complex. In both scenarios, we noticed a significant inhibition of the dissipation of $\Delta\Psi_m$ upon As_2O_3 treatment (Figure 2g and Supplementary Figure S2e). Calcein staining, a commonly used assay for the PT-pore, indicated the activation of the protein complex and we have also observed the release of cytochorome c (Supplementary Figure 2f,g). These results suggested a signaling pathway induced by As_2O_3 from complex II disintegration, the formation of ROS and the activation of the PT-pore for cell death.

Ca^{2+} influx by ionomycin induces complex II disintegration for cell death induction. When compared with As_2O_3, Ca^{2+} influx into mitochondria with ionomycin, a Ca^{2+}-specific ionophore, was more efficient, (Figure 1a). It likewise caused the disintegration of complex II (Supplementary Figure S3a), which was reversed by the expression of PHB (Figure 3a). This complex II assembly factor also specifically reduced ROS and cell death by ionomycin (Figures 3b and c and Supplementary Figure S3b). The incubation of isolated complex II in Ca^{2+}-containing buffer led to the release of the SDHA/SDHB sub-complex as observed in blue native gel electrophoresis (Supplementary information, Supplementary Figure S3c). To more directly address the mechanism of Ca^{2+}-mediated complex II disintegration, we reconstituted complex II from mitochondrial membranes into nanoscale bilayers (nanodiscs) as described.[21] Complex II reconstituted in bilayers with an inner membrane-biomimetic lipid composition (palmitoyloleoylphosphatidylcholine, POPC; palmitoyloleoylphosphatidylethanolamine (POPE); and cardiolipin (CL) in a 2:2:1 molar ratio) displayed a Ca^{2+}-dependent release of SDHA, whereas complexes lacking the dimeric phospholipid CL (POPC and POPE in equimolar concentrations) displayed no such Ca^{2+}-coupled disintegration (Figure 4a). Consistent with this trend, succinate:ubiquinone oxidoreductase activity, which requires an intact holoenzyme, was reduced in a Ca^{2+}-dependent manner for complexes in the presence of cardiolipin, supporting the specific disintegration of complex II (Figure 4b).

To further ensure that the cellular effects observed upon Ca^{2+} influx were caused by complex II dissociation, we blocked the enzymatic activity of complex II using malonate as

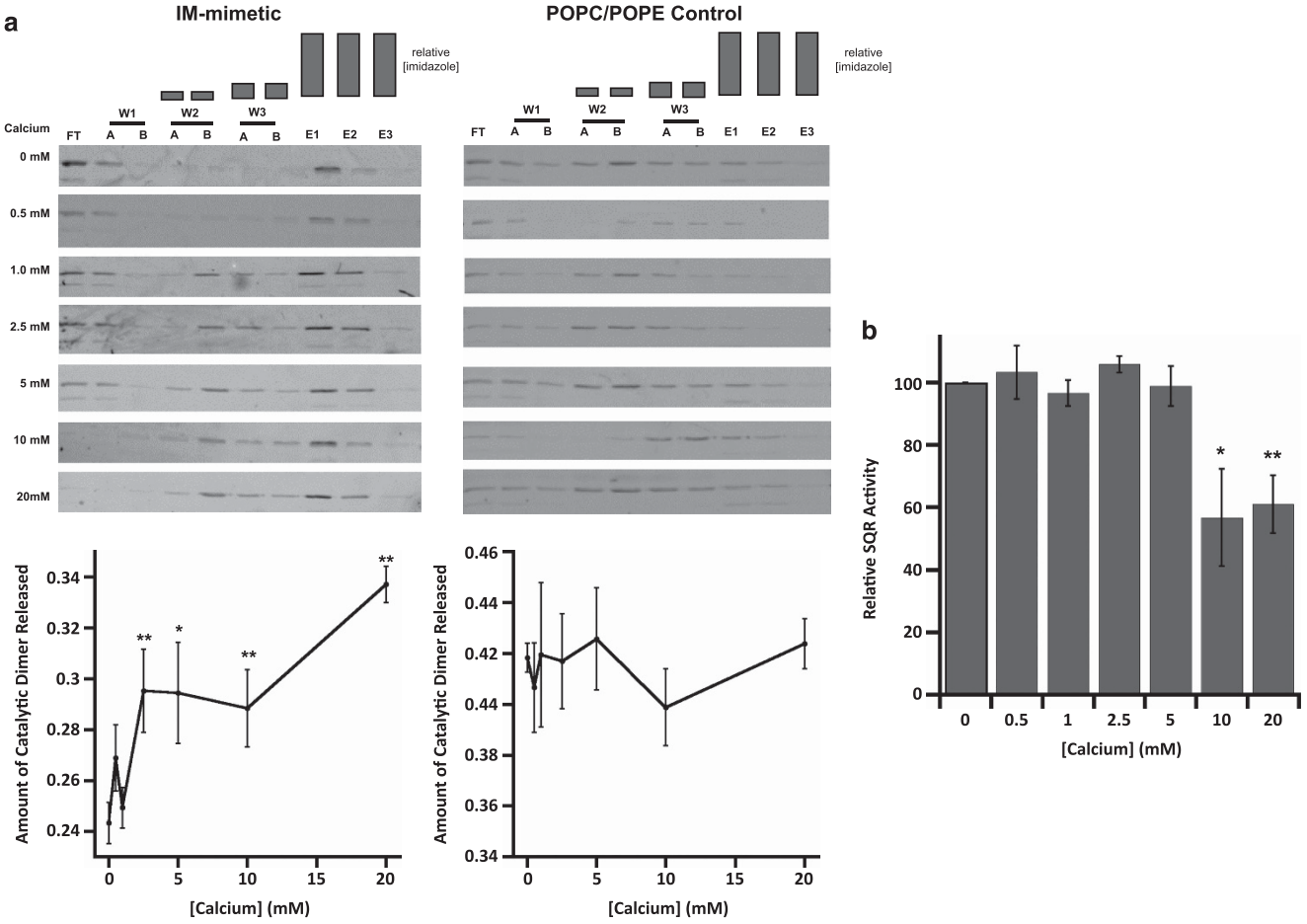

Figure 4 Cell-free system upon Ca^{2+} addition. (**a**) Complex II was reconstituted into nanodiscs containing cardiolipin (IM-mimetic) or lacking cardiolipin (POPC/POPE Control), incubated with the indicated concentrations of Ca^{2+}, then subjected to Ni-NTA affinity chromatography along with an imidazole gradient. Subunits co-eluting with the nanodisc scaffolding protein (MSP1E3D1) in fractions E1 and E2 were stably associated with the nanodiscs; subunits emerging from the column at earlier fractions were not stably associated. (upper panels) SDS-PAGE analysis of the column fractions. The fluorescent FAD signal was used as a marker for the soluble catalytic dimer as FAD is covalently bound to Sdh1p. FT: flow through; W1A-W3B: wash steps; E1-E3 elution steps. (lower panels) Quantification of FAD band intensity comparing the predominant middle Wash fraction (W2B in most cases or W3A under some conditions) and combined selected Wash with E1 and E2 (which represents the total of the catalytic dimer in the predominant wash and all that remains connected to the membrane dimer within nanodiscs). A larger ratio indicates a less stable complex (i.e. more catalytic dimer is not stably associated with nanodiscs and washes off the column prior to E1 and E2). Error bars are representative of S.E.M. for at least three separate experiments and statistical differences are represented in relation to addition of 0 mM Ca^{2+} ($*P \leq 0.05$; $**P \leq 0.01$). (**b**) The SQR activity of complex II is Ca^{2+}-dependent. Succinate: quinone oxidoreductase (SQR, DB-mediated) activity monitoring the presence of the holoenzyme is Ca^{2+}-dependent reflecting the decreased affinity between the catalytic and membrane dimers. Error bars are representative of S.E.M. for at least four separate experiments and statistical differences are represented in relation to addition of 0 mM Ca^{2+} ($*P \leq 0.05$; $**P \leq 0.01$)

well as 3-NP. The cellular parameters that could be lowered by PHB (Figures 3b and c), the formation of ROS and subsequent cell death, were specifically reduced (Figures 5a and b and Supplementary Figure S4a). The importance of oxidative stress for ionomycin-induced cell death was further emphasized by the increased survival when ROS were squelched by the expression of mitochondrial MnSOD (Figure 5c). When we blocked the PT-pore with knocked-out or overexpressed cypD, we observed a reduction of cell death (Figure 5d and Supplementary Figure S4b). Transfection of MCU, the mitochondrial Ca^{2+} uniporter, induced cell death that could be inhibited with 3-NP (Supplementary Figure S5a). To further strengthen the case for an involvement of mitochondrial Ca^{2+} influx and PT-pore activation being responsible for As_2O_3-induced cell death, we tested the Ca^{2+} chelator BAPTA, the uncoupler FCCP and also the PT-pore inhibitor cyclosporine A. All three reagents could reduce cell death induced by As_2O_3 (Supplementary Figure S5b,c). Moreover, ruthenium red, the inhibitor of the mitochondrial Ca^{2+} uniporter, diminished the FRET reduction upon As_2O_3 treatment and increasing the As_2O_3-concentration also enhanced the reduction of the FRET effect (Supplementary Figure S5d,e).

Cardiolipin depletion activates complex II for cell death induction. Under our cell death conditions, cardiolipin levels, which is highest in mitochondria (Supplementary Figure S6a,b), remained unchanged (Supplementary Figure S6c-h). The headgroup of this lipid has been shown to bind Ca^{2+}, which induces those lipids to coalesce into detached

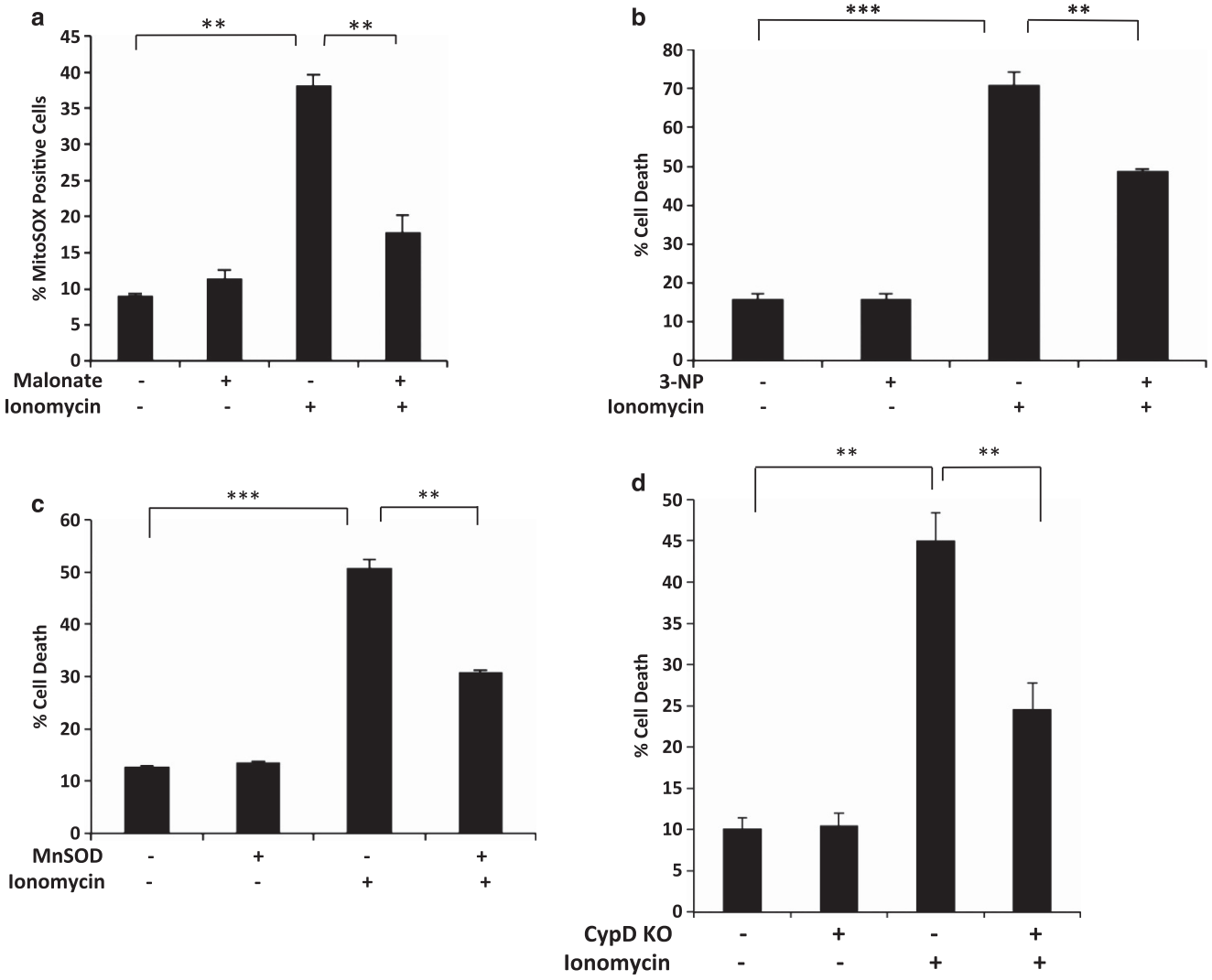

Figure 5 The cellular effects of ionomycin-mediated Ca^{2+} influx depend on complex II, ROA, and the PT-pore. (**a**) HeLa cells were left untreated or treated for 8 h with 10 μM ionomycin, with or without 8 mM malonate, and harvested for MitoSOX stain with FACS analysis to determine ROS generation in each sample. (**b**) HeLa cells were treated for 24 h with 10 μM ionomycin with or without 1 mM 3-NP and then harvested for $DiOC_6$ and PI stain with FACS analysis. The FACS results were used to determine the percent cell death within each sample. (**c**) HeLa cells were transfected with pcDNA3 as a control or Manganese superoxide dismutase (MnSOD) 24 h prior to treatment with 10 μM ionomycin for 20 h and harvested for $DiOC_6$ and PI stain with FACS analysis. The FACS results were used to determine the percent cell death. (**d**) WT and CypD knockout MEF cells were treated for 16 h with 10 μM ionomycin and harvested for FACS analysis to determine the percent cell death present within each sample. $^{**}P<0.01$, $^{***}P<0.001$ (student's *t*-test)

homotypic clusters and exhibit lateral phase separation, thereby causing an immobilization of cardiolipins[22] and reducing their interaction with respiratory chain complexes.[23] We therefore investigated the cellular consequences when complex II association with cardiolipin is reduced and targeted the expression of cardiolipin synthase-1 (CLS1) in the inner mitochondrial membrane (Supplementary Figure S6i-l). This led to a reduction of the FRET ratio indicating a disintegration of complex II (Supplementary Figure S6m) prior to the accumulation of overt cell death (Supplementary Figure S6n). The effect on FRET between SDHB and SDHD could be reversed by the transfection of PHB (Figure 6a). In line with complex II being activated by CLS1 knock-down, ROS were produced, which could likewise specifically be reduced by PHB expression (Figure 6b and Supplementary Figure S3b), as was the induction of cell death by CLS1 knockdown (Figure 6c). The complex II-specific inhibitor 3-NP reduced both ROS and cell death by CLS1 knockdown (Figures 6d and e). MnSOD transfection supported the role of ROS in this scenario, whereas this enzyme had no effect on cell death induced by the caspase-2 control indicating its specificity (Figure 6f, Supplementary Figure S7). To also test the involvement of the PT-pore in the signal created by the absence of cardiolipin, we knocked down CLS1 in WT and in cypD KO cells and observed a significant reduction of cell death in the absence of cypD (Figure 7a and Supplementary Figure S8a–f). Transfection of the cells with a plasmid for cypD likewise led to cell death reduction (Supplementary Figure S8g). Finally, to test whether cardiolipin content is the limiting factor for cell death induction, we upregulated CLS1,

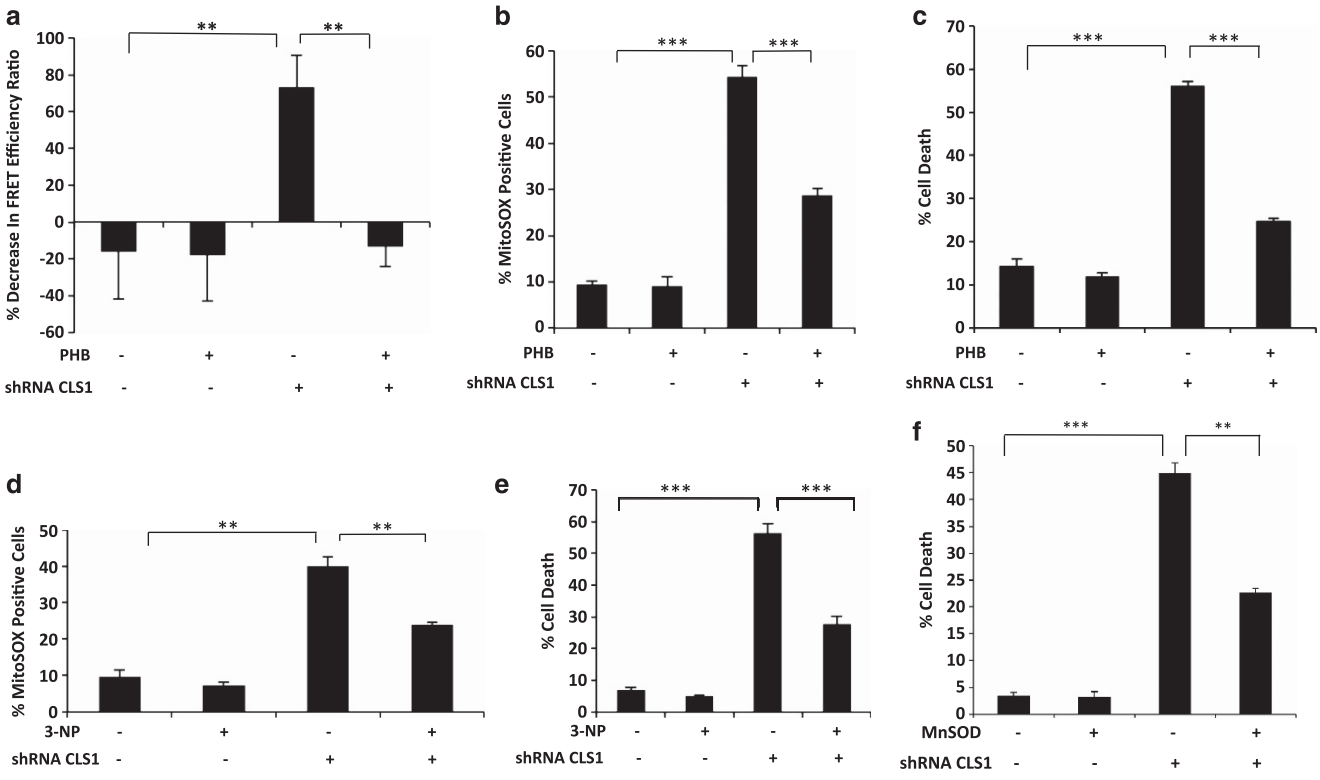

Figure 6 Removal of cardiolipin disintegrates complex II for ROS formation and cell death induction. (**a**) HeLa cells were co-transfected with a scrambled shRNA or an shRNA against CLS1, together with pcDNA3 or an expression plasmid for PHB. An initial measurement for FRET efficiency was made in triplicates for all four sets immediately following the transfections and 24 h post co-transfection. Data are represented as in Figure 1d. (**b**) HeLa cells were transfected with a scrambled shRNA or an shRNA against CLS1, together with either pcDNA3 or an expression plasmid for PHB at a 1 : 1 ratio. The cells were harvested for MitoSOX 48 h post transfection to determine ROS. (**c**) HeLa cells were transfected with a scrambled shRNA or an shRNA against CLS1, together with either pcDNA3 or PHB at a 1 : 2 ratio. The cells were harvested for $DIOC_6$ and PI stain to quantify cell death 72 h post transfection. (**d**) HeLa cells were transfected with a scrambled shRNA or an shRNA against CLS1 and harvested for MitoSOX stain 48 h post transfection with 3-NP treatment 8 h prior to harvest. (**e**) HeLa cells were transfected with a scrambled shRNA or an shRNA against CLS1. The cells were harvested for $DIOC_6$ and PI staining to quantify cell death 72 h after transfection with 3-NP treatment 24 h prior to harvest. (**f**) HeLa cells were transfected with shRNA SCR or shRNA CLS1 together with pcDNA3 or MnSOD (2 : 1 ratio). 72 h post transfection the cells were harvested for FACS analysis

which caused a pronounced increase of its product and a significant reduction of cell death by As_2O_3 and ionomycin (Figures 7b and c and Supplementary Figures S8h–k).

Discussion

In this work, we showed that massive mitochondrial Ca^{2+} influx causes complex II disintegration for ROS formation and cell death induction. The agonist-releasable Ca^{2+} concentration in the ER is in the mM range[24] and high sub-mM concentrations still mediate physiological responses in mitochondria.[25] Hence, only when a considerable amount of this ion accumulate in mitochondria is cell death induced. This is facilitated through the close apposition of the ER with mitochondria or the massive influx of the ion from the extracellular space. For our findings to be relevant for cell death caused by mitochondrial Ca^{2+} accumulation, complex II should respond only to very high Ca^{2+} concentrations as observed in Figure 4a. Ca^{2+} has a high affinity to cardiolipin with a kD in the μM range,[26] making it likely that it is the abundance of this lipid in the inner mitochondrial membrane that limits its efficient removal from complex II.

We note that the range of [Ca^{2+}] used in our *in vitro* experiments is higher than the levels of free mitochondrial Ca^{2+} reported in the literature and measured in cells (Supplementary Figure 1a). It should, however, be emphasized that the important measure in our assays is not the absolute concentration of Ca^{2+}, but rather the molar ratio of Ca^{2+} to lipid in the experimental system. Thus, at a Ca^{2+} concentration of 1 mM, where we begin to see effects on complex II stability and activity, the molar ratio of Ca^{2+} to cardiolipin is $\sim$4 : 1. We note that the model membranes used in these assays contain a physiologically relevant cardiolipin concentration (20 mol%). Although titrating down the cardiolipin amounts would in principle lower the threshold [Ca^{2+}] at which we detect a response, we have found that lowering the cardiolipin concentration in these bilayers results in decreased complex II stability and activity. Also relevant to this point, we note that it is difficult to obtain consistent measurements of free Ca^{2+} levels within mitochondria owing to pH effects and interference by heavy metal ions. Moreover, high Ca^{2+} levels are likely generated in the proximity of Ca^{2+} channels of the inner membrane (IM) where complex II is localized. This effect is not captured by the Ca^{2+} measurements currently employed, which monitor the total ion concentration in the mitochondrial matrix. In support of our model, modulating the cardiolipin level determined the sensitivity to cell death induction. Its increase reduced cell

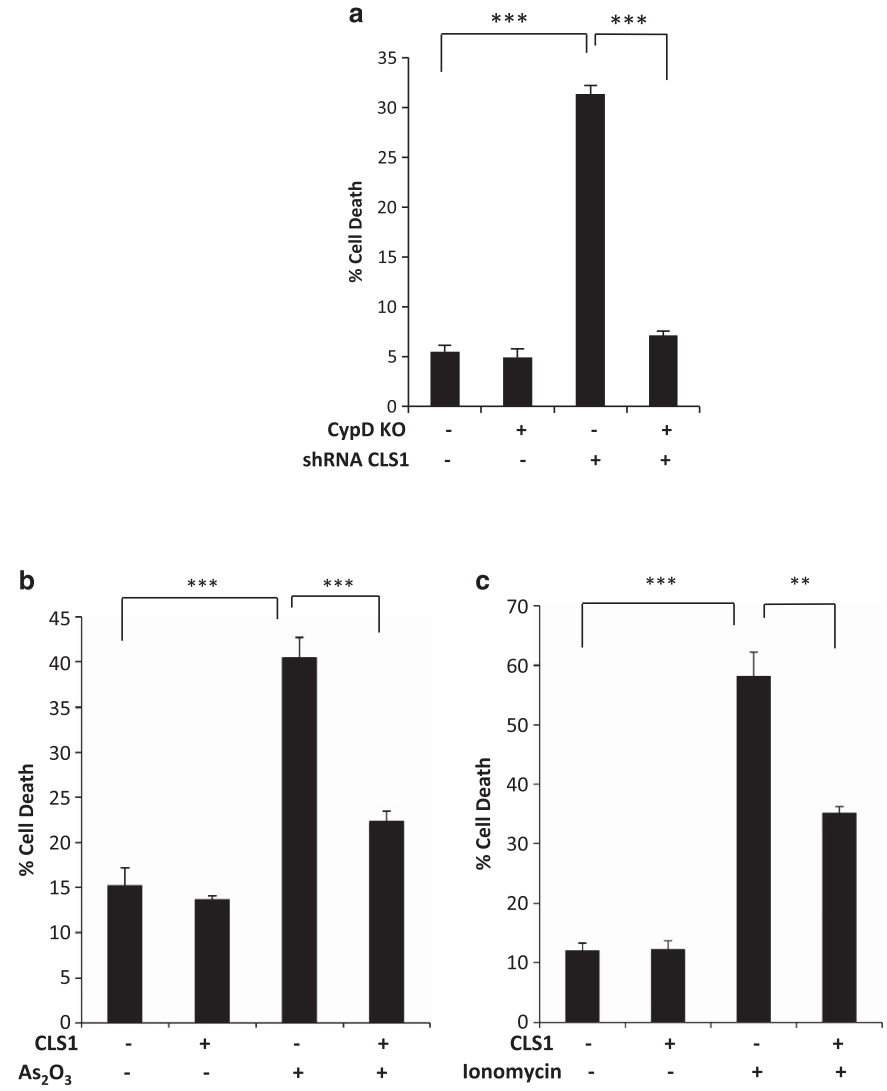

Figure 7 Cardiolipin reduction correlates with PT-pore activation and cardiolipin increase reduces cell death. (**a**) WT and cypD knockout MEF cells were transfected with shRNA SCR or mouse shRNA CLS1 and harvested for $DiOC_6$ and PI staining with FACS analysis after 72 h to determine the percent cell death present within each sample. (**b**) HeLa cells were transfected with pcDNA3 as a control or CLS1 24 h prior to treatment, then treated for 25 h with 10 μM As_2O_3 and harvested for FACS analysis to determine the percent cell death present within each sample. (**c**) HeLa cells were transfected with pcDNA3 as a control or CLS1 24 h prior to treatment, then treated for 20 h with 10 μM ionomycin and harvested for FACS analysis to determine the percent cell death present within each sample. $^{**}P<0.01$, $^{***}P<0.001$ (Student's *t*-test)

death (Figures 7b and c), whereas its reduction activated complex II for ROS formation and the demise of the cell (Figures 6a–c). The binding of Ca^{2+} to cardiolipin has previously been implicated in ROS formation without the identification of a specific cellular process.[27] Although we cannot exclude more indirect effect on the physiology of mitochondria and eventually on cell death when we target the CLS1, cardiolipin's role in cell death has been acknowledged with both pro- and anti-survival functions depending on its subcellular localization.[28] It can act as the mitochondrial receptor for BID,[10] oligomerizes the multidomain proapoptotic BAK and BAX molecules,[11] and retains cytochrome C in the cristae of mitochondria from which it is released upon oxidation.[12] One recent study observed that the reduction of cellular cardiolipin content to 25% of its normal level by targeting CLS1 led to an increased sensitivity for apoptosis,[29] whereas another publication with a more modest reduction of the lipid observed the opposite cellular effect.[30] In both experiments, stable cell clones were used, which could have introduced a selection bias. Mutations in tafazzin (Taz1p), a cardiolipin transacylase, have been shown to cause the X-linked Barth syndrome. Such cells show a reduced cell death in the type II response to Fas receptor activation.[31] However, these cells still contain cardiolipin as Taz1p only chemically modifies the lipid.

We used FRET constructs of SDHB and SDHD in our study to monitor the dissociation of complex II subunits for cell death induction. We discount the possibility that the fluorescent proteins themselves are effecting a spurious interaction between the subunits because: (i) In the absence of correct assembly, SDHB, SDHC, and SDHD are degraded.[9] Any potential EYFP-CFP mediated complex between the fusion proteins with SDHB and SDHD, in the absence of productive complex II formation, would, therefore, be expected to be

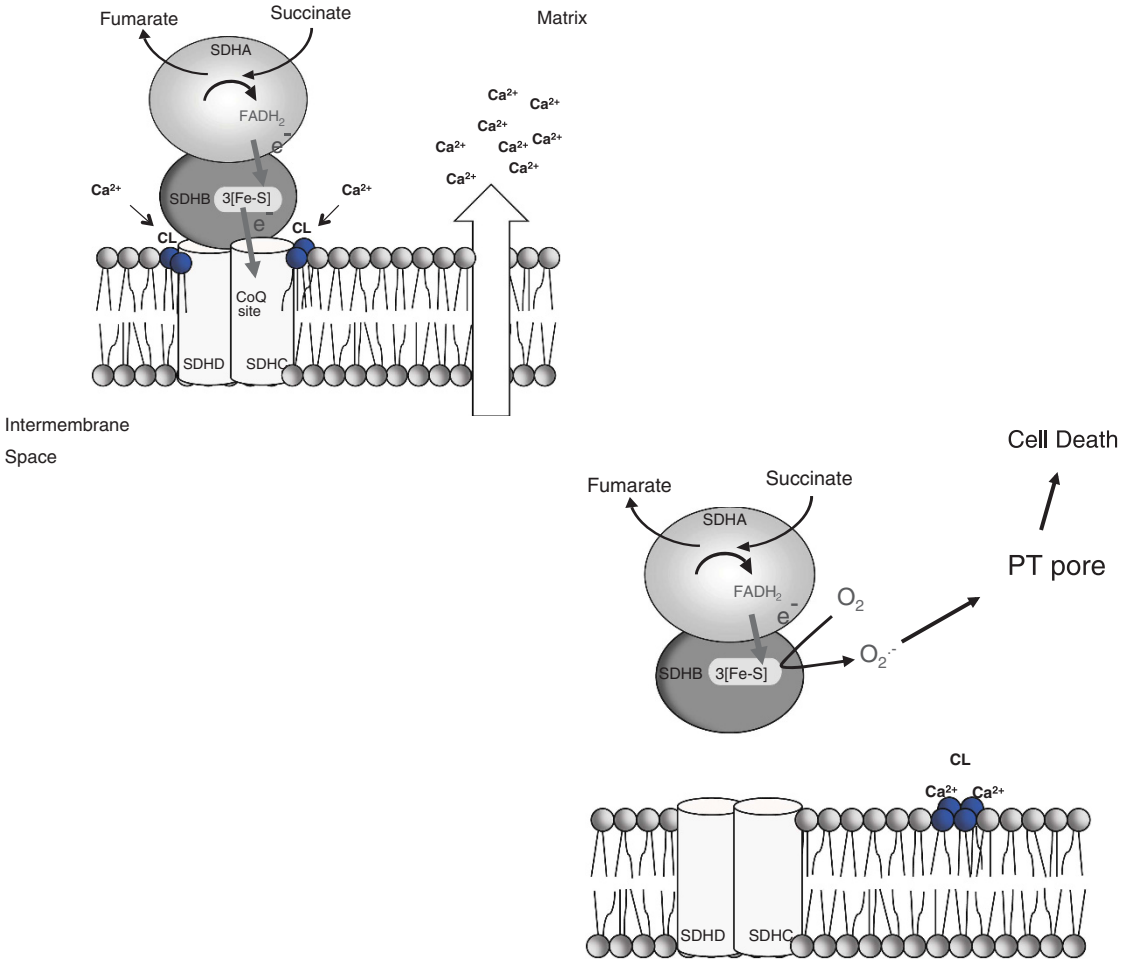

Figure 8 Signal cascade involving Ca^{2+}, cardiolipin, complex II, ROS and, the PT-pore for cell death. Upon influx of Ca^{2+} into the matrix of mitochondria the ions bind CL (left panel), which leads to its dissociation from complex II that releases the enzymatically active SDHA and SDHB subunits. As a result, ROS are generated that activate the PT-pore for cell death (right panel)

degraded, which is not what we see. (ii) The presence of SDH-specific chaperone PHB restores the FRET signal (Figure 2a). Taken together, these results support the use of the FRET constructs as a noninvasive way to monitor the associations of the catalytic dimer with the membrane-anchoring subunits.

In contrast to the instability of the components of complex II, when one of them is missing,[9] sub-complex of SDHA and SDHB seems to be stable, even during cell death induction (Supplementary Figure S1i). Hence, the complex behaves differently when its assembly is disturbed or when it specifically releases the SDHA/SDHB sub-complex for cell death induction. Clearly, the mechanism of how the complex is assembled, including the exact function of PHB, requires further investigation. In addition to the disintegration for cell death induction, we also observed an increase in FRET during nonlethal stress such as transfection and prolonged incubation after exposure to the confocal microscope potentially induced to counteract the stress (Supplementary Figure S1h). This indicates that the disintegration and assembly of complex II is dynamic and responds differentially to lethal and manageable cellular stress.

Although mitochondrial Ca^{2+} overload has been described for As_2O_3,[32] possibly as a result of ER stress,[33] it has most prominently been associated with cell death in response to ischemia-reperfusion of the heart and with excitotoxicity of neurons. The PT-pore has been regarded in those pathological scenarios as the target for increased mitochondrial Ca^{2+} as its inhibition by bongkrekic acid and cyclosporin A results in a reduction of Ca^{2+}-induced cell death.[34] However, in the absence of a generally accepted structure for the PT-pore complex, how directly or indirectly this is accomplished is unknown and the identification of alternative targets for mitochondrial Ca^{2+} such as complex II is critical to explain the effects of this ion. Our data indicate that the cyp -sensitive PT-pore is eventually activated for cell death by the disintegration of complex II. This protein structure has been implicated in necrotic and apoptotic cell death,[19,20] in line with our observation that both necrosis and apoptosis are caused by CLS1 knockdown, As_2O_3, and ionomycin. PT-pore activation by Ca^{2+} has been described to require additional stimuli for full activation, but it was later recognized that a substantive Ca^{2+} influx into mitochondria can suffice to generate ROS and activate the PT-pore.[34–36] Although formally we cannot exclude additional, parallel pathways such as the activation of Bax/Bak or the involvement of other complexes of the respiratory chain,[37–39] we observed that complex II activation

by Ca^{2+} caused ROS formation and the specific complex II inhibitors 3-NP and malonate reduced ROS formation and cell death by ionomycin, As_2O_3 and CLS1 knockdown (Figures 2d and e, Figures 5a and b, Figures 6d and e).

Our data lay out a signaling pathway from mitochondrial Ca^{2+} influx that targets cardiolipin, to complex II disintegration, ROS formation, and PT-pore activation for cell death (Figure 8). Our findings will lead to more specific interference options in the numerous pathological scenarios that are connected with massive mitochondrial Ca^{2+} influx.

Materials and Methods

Cell culture and reagents. HeLa and HEK293T cells were cultivated in DMEM (Sigma, Gillingham, Dorset, UK) supplemented with 10% FCS (Invitrogen, Paisley, UK), 2 mM L-glutamine (Invitrogen), 2 mM sodium pyruvate (Invitrogen), penicillin (100 U/ml), and streptomycin (100 mg/ml). Lipids were obtained from Avanti Polar Lipids (Alabaster, AL, USA). All other chemicals were purchased from Sigma-Aldrich (St. Louis, MO, USA) or Thermo Fisher Scientific Inc. (Pittsburg, PA, USA).

Plasmid vectors and transfections. All plasmid vectors used were cloned into the pcDNA3 vector (Invitrogen) unless otherwise stated. The expression plasmids for CypD and MnSOD have been described.[18,40] The PHB plasmid was constructed using PCR amplification and subcloning techniques involving PhusionTM DNA polymerase (Thermo Fisher Scientific, Cramlington, UK) and was also subcloned into pcDNA3. The FRET acceptor (YFP-SDHB fusion protein) was constructed using PCR amplification and subcloning techniques involving PhusionTM DNA polymerase (Thermo Fisher Scientific) with the following sets of primers: 5′-ACTCTCGAATTCGCCGCCACC ATGGCGGCG-3′ (SDHB, forward) and 5′-CTCGCCCTTGCTCACCATACCACCAGAACCACCAAC TGAAGCTTTCTTCTCCTT-3′ (SDHB, reverse), 5′-GAGAAGAAAGCTTCAGTTGG TGGTTCTGGTGGTATGGTGAGCAAGGGC-3′ (YFP, forward) and 5′-GAAGA TGCGGCCGCCTAGCCGAGAGTGATCCC-3′ (YFP, reverse). The FRET donor (CFP-SDHD fusion protein) was constructed using PCR amplification and subcloning techniques involving PhusionTM DNA polymerase (Thermo Fisher Scientific) with the following sets of primers: 5′-ACTCTCGAATTCGCCGCCACC ATGGCGGTTCT-3′ (upper SDHD, forward) and 5′-CTCCTCGCCCTTGCTC AACAT TGCAGCCTTGGAGC-3′ (upper SDHD, reverse), 5′-CACCATTCTGGCT CCAAGGCTGCAATGTTGAGCAAGGGCG-3′ (CFP, forward) and 5′-CTTGGA GCCAGAACCACCAGAACCACCGGCGGCGGTCAC-3′ (CFP, reverse), 5′-ACCG CCGCCGGTGGTTCTGGTGGTTCTGGCTCCAAGGCT-3′ (SDHD, forward) and 5′-GAAGATGCGGCCGCCTAGAGCTTCCACAGCATG-3′ (SDHD, reverse). The peptide linker GGSGG (ggtggttctggtggt) was inserted in the fusion site of both FRET constructs to allow flexibility of the spatial separation for the GFP variants. EcoRI and NotI were the inserted restriction sites for cloning into the pcDNA3 vector. shRNA for cardiolipin synthase (CLS1) was purchased as a MISSION shRNA bacterial glycerol stock (Sigma, NM-019095). Effectene or jetPEI were used to transfect plasmid DNA into HeLa or HEK293T cells, respectively.

Mitochondria isolation. Mitochondria were isolated either with a commercial isolation kit (Pierce, Thermo Fisher Scientific) or with established protocols,[41] resuspended in a buffer (20 mM HEPES pH 7.4, 1 mM EGTA, 1 mM EDTA, 1.5 mM $MgCl_2$, 10 mM KCl, 0.25 mM sucrose, complete protease inhibitor) and kept at $-80\,^{\circ}C$.

Western blotting. For each sample, a Bradford assay was done to quantify the amount of protein, then mitochondrial proteins (3–20 μg, depending on experiment) were separated in a 14% SDS-PAGE and electroblotted onto nitrocellulose membranes (Bio-Rad, Hemel Hempstead, UK), which were processed as described (Lemarie A, Grimm S, 2009). Mouse monoclonal antibody against cytochrome C was purchased from BD Pharmingen (Oxford Science Park, UK); Rabbit polyclonal antibody against human cardiolipin synthase (CLS1) was purchased from Source Bioscience (Seattle, WA, USA); Mouse monoclonal antibodies against SDHA and GAPDH and rabbit polyclonal antibodies against GRP75 and COX IV, subunit 4 were purchased from Santa Cruz Biotechnology (Heidelberg, Germany); the respective HRP-conjugated secondary antibodies were from Invitrogen.

Blue native gel PAGE. For the *in vitro* Ca^{2+} experiments, fresh mitochondria isolated using the commercial isolation kit were incubated in the indicated buffers. Mitochondrial complex II was gently solubilised in a 50 mM Bis–Tris buffer containing 5–8% (wt/vol) *n*-dodecyl-maltoside and 750 mM 6-aminocaproic acid on ice for 30 min and the supernatant collected after centrifugation (20 000 $\times$ *g*, 30 min). This protocol retains the integrity of the respiratory chain complexes.[42] Native Sample Buffer (Bio-Rad), supplemented with 1.25% (w/v) (final concentration) Coomassie brilliant blue G solution (5% coomassie brilliant blue G, 750 mM 6-aminocaproic acid, and 50 mM Bis–Tris) was added to the supernatants. Proteins were loaded on a Ready-Gel 4–15% (Bio-Rad) for Blue Native Page and western blot was performed according to established protocols. Blots were probed with an SDHA antibody (Invitrogen).

FRET efficiency imaging and calculation. Adducts of GFP variants have been widely used to monitor protein and membrane associations of numerous proteins.[43] FRET was assessed using the YFP-SDHB acceptor and CFP-SDHD donor fusion proteins with the Leica TCS SP5 Confocal and its respective FRET Sensitized Emission Wizard. HeLa and HEK293T cells were infected with viral plasmids expressing the fusion proteins to generate stable clones for the FRET experiments. The FRET efficiency was calculated using the Leica protocol detailing a specific equation $E_A(i) = (B\text{-}A^*\beta\text{-}C^*\gamma)/C$ where $E_A(i)$ is the apparent FRET efficiency, whereas A, B, and C correspond to the intensities of the 3 signals (donor, FRET, and acceptor) and α, β, and γ are the calibration factors generated by acceptor only and donor only references. Cells stably expressing donor signal alone, donor and acceptor signals, and acceptor signal alone were used in an image acquisition process, which optimized donor, FRET, and acceptor channels, respectively, based on expression levels. The donor and FRET channels were defined first by the simultaneous excitation and detection of the donor and acceptor (donor = CFP excitation 458 nm; emission 462–510 nm; acceptor = YFP excitation 514 nm; emission 518–580 nm). This enabled the assessment of the fluorescence intensities, PMT gain, and laser dose for each channel. Next, the laser light of the acceptor was reduced to 0% to enable excitation selectively for the donor in order to properly define conditions for the donor and FRET imaging. The acceptor channel was likewise defined by reducing the donor excitation light down to 0% (the step by step protocol can be found at: https://workspace.imperial.ac.uk/imagingfacility/public/Leica-FRET_SE-Application_Letter_20.EN.pdf). In experiments looking at the effect of complex II inducers (As_2O_3, ionomycin, and CLS1 knockdown) and the inhibitor PHB, an average set of six start measurements of FRET efficiency were made along with an average set of six end measurements and normalized to a set of measurements done on fixed cells in 4% formaldehyde. The ratios of the FRET efficiencies were used to calculate the percent change.

Quantification of cell death. The mitochondrial depolarization was quantified using $DiOC_6$ (Sigma-Aldrich, 40 nM) and counter stained with propidium iodide (PI; 6 mg/ml) in phosphate-buffered saline (PBS). Cells were incubated for 90 min before analysis. Quantification was set at 5 000 for cell count and FL1 (530 nm) and FL3 (670 nm) were used to acquire $DiOC_6$ and PI signals, respectively. Sample data were acquired using flow cytometer (BD Biosciences, San Jose, CA, USA) and analyzed with the FlowJo programme (TreeStar Inc., Ashland, OR, USA). The bar graphs are normalized to percent transfection efficiency by subtracting or adding, depending on if we are looking at inhibition or induction, the difference between the data from the experimental condition and the background control, then multiplying the result by the quotient of 100% and the percent transfection efficiency.

ROS detection. The ROS-sensitive probe MitoSOX was used according to a previously published protocol (Lemarie *et al.*, 2010). Briefly, cells were treated with the indicated conditions, harvested, and washed in PBS before the addition of 150 ml of a PBS solution containing MitoSOX (5 mM). Cell were incubated at $37\,^{\circ}C$ for 10 min and then washed and resuspended in PBS. Fluorescence was measured by flow cytometry using a FACScalibur (FL2-H channel) and a minimum of 5 000 cells were counted for each sample.

Mitochondrial calcium measurement. Cells were harvested and resuspended in PBS (without $CaCl_2$ supplement) containing 1.0 mg/ml of Rhod-2/AM (Molecular Probes, Invitrogen) for 45 min in the incubator ($37\,^{\circ}C$) with frequent agitation. Cells were then washed and resuspended in PBS for FACS acquisition (BD Biosciences). The FACS results were all gated using the same

settings, so the differences between percent mitochondrial calcium levels are comparable. The FL2 channel was used for the gating of the Hela cell population that was shifted to the right on the FL2 axis after Rhod-2-AM-staining with As_2O_3 or ionomycin treatment.

Cardiolipin quantification. The human cardiolipin IgG (human antibody against cardiolipin) was purchased from ImmunoVision (Springdale, AR, USA) (HCL-0100) and the secondary Alexa Fluor 488 goat anti-human IgG was purchased from Invitrogen (A11013). The standard protocol for immunofluorescence staining for FACS was used. The harvested cells were incubated in TBSS (0.02% saponin, 1xTBS) for 30 min at 37 °C to permeabilise them, then blocked in 3% BSA TBSS solution for 30 min at 37 °C. Afterwards, the cells were stained in 1 : 500 dilution in TBSS of the primary antibody against cardiolipin for 30 min at 37 °C, washed with PBS, and stained in 1 : 500 dilution in TBSS of the secondary antibody against human IgG. Sample data were acquired using flow cytometer (BD Biosciences) and analyzed with the FlowJo programme (TreeStar Inc.).

Viral production. The FRET constructs were cloned into 3rd generation lentiviral vectors (kind gift from Prof Nicholas Mazarakis, Imperial College) containing a cPPT (central polypurine tract) and WPRE (Woodchuck hepatitis posttranscriptional regulatory element) sequences. Cloning was done using the IN-FUSIOn technology from Clontech and viral production was done using standard techniques. Briefly, 293T cells were transfected with packaging plasmids and the transfer vector plasmid containing the gene of interest using the calcium phosphate transfection protocol. Forty-eight hours post transfection, virulent supernatants were collected and either frozen or used directly to transduce target cells.

Assembly of nanodiscs. Mitochondria were isolated from *Saccharomyces cerevisiae* (strain D273-10B) as previously described,[44] and stored in 2 mg aliquots at −80 °C until use. Aliquots were thawed on ice for 10 min and subsequently solubilized in buffer (50 mM potassium phosphate (pH 7.4), 50 mM KCl) with DDM at a final detergent:mitochondrial protein ratio of 1.5 : 1.0 g (~2% (w/v) DDM). Samples were incubated for 25 min at RT and then subjected to a clarifying centrifugation spin to remove any non-solubilized materials. The supernatant containing solubilized mitochondrial proteins was used in nanodisc assembly. POPC/POPE control lipid mix (50 : 50 mol%) or IM-mimetic lipid mix (POPC, POPE, and cardiolipin in 40 : 40 : 20 mol%) in chloroform were dried under a N_2 stream and desiccated under vacuum overnight to remove organic solvents, as described.[45] Lipids were reconstituted in membrane scaffolding protein (MSP) buffer (20 mM Tris-HCl (pH 7.4), 100 mM NaCl) with 59 mM sodium cholate and bath sonicated to resuspend. MSP (MSP1E3D1) was synthesized and purified as described.[46] Lipid mixes, MSP1E3D1 (in lipid: MSP ratios of 140 : 1), DDM-solubilized mitochondrial proteins, and MSP buffer (with 14.8 mM cholate) were incubated at RT for 30 min. Samples were added to pre-hydrated Bio-Beads SM Hydrophobic Interaction Adsorbent (Bio-Rad Laboratories Inc., Hercules, CA, USA) and rotated at RT for 2 h. This process removed detergent from the sample and allowed nanodisc self-assembly to occur. At the end of 2 h, samples were removed from Bio-Beads and prepared for subsequent analysis.

Complex II affinity assay. Samples were dialyzed into MSP buffer without NaCl in Centricon 3000 MWCO tubes in an Eppendorf Centrifuge 5804R and then split into three separate samples that were then subject to addition of various concentrations of calcium (Ca^{2+}) as $CaCl_2$ ((final) = 0, 0.5, 1, 2.5, 5, 10, 20 mM). Samples were rotated for 15 min at RT and then added to Ni-NTA agarose and further rotated for 40 min at RT. After nanodiscs were subjected to step gradients of MSP buffer and imidazole (up to 400 mM) to isolate the nanodiscs through the His-tagged MSP1E3D1, samples were taken from each fraction that emerged from the column and analyzed via 12% SDS-PAGE for the presence of FAD. Gels were scanned on a Bio-Rad Pharos FX Plus Molecular Imager with external lasers using Quantity One software (version 4.6.9) under the FITC fluorescence setting (488 nm laser, 530 nm emission filter) in order to detect the FAD signal from Sdh1p (yeast SDHA). The stronger, higher MW band represents FAD-Sdh1p and the lower migrating bands represent other mitochondrial flavoproteins.[47] Affinity assay data are represented as the band intensity of the predominant middle wash fraction (in most cases Wash 2B) compared with the band intensity of this wash fraction combined with Elutions 1 and 2, which represent fully assembled nanodiscs.

Cell fractionation. Freeze thaw was used with liquid nitrogen on the pellet suspended in mitochondrial lysis buffer (12 ml Buffer A (20 mM HEPES pH 7.5, 1.5 mM $MgCl_2$ ($6H_2O$), 10 mM KCl, 1 mM EDTA, pH 7.4) with 3 ml sucrose 1.25 M). The samples are frozen using 15-s submersions in liquid nitrogen and left to thaw at room temperature. This is repeated four more times before centrifugation at 20 000 RPM for 30 min to pellet non-matrix membrane components.

Complex II activity assays. Samples were incubated with Ni-NTA agarose while rotating for 40 min at RT immediately after removal from Bio-Beads. They were subjected to the same step gradients as the affinity assay samples (see Complex II Affinity Assay, above) and the first two elution fractions, which contain the nanodiscs, were combined, dialyzed to remove imidazole and concentrated in Centricon 3000 MWCO tubes in the Eppendorf Centrifuge 5840R. After dialysis/concentration, nanodiscs were split into six separate samples and incubated with various concentrations of calcium (Ca^{2+}) as $CaCl_2$ ((final) = 0, 0.5, 1, 2.5, 5, 10, 20 mM) for 15 min at RT. Samples were then ready for activity assay analysis. Assays were conducted as previously described[48] on an Amersham Biosciences Ultrospec 2100 pro UV/Vis Spectrophotometer in 1 cm plastic cuvettes following extinction of DCPIP absorbance ($\varepsilon_{600} = 20.7\ mM^{-1}\ cm^{-1}$). For SDH activity (PMS-mediated) measurements, master mix (50 mM Tris (pH 7.5), 5 mM succinate (pH 7.5), 0.5 mM DCPIP, 0.1 mM PMS) was added to the samples, and they were then incubated for 8 min prior to measurements. For SQR activity (DB-mediated) measurements, samples were pre-incubated with 10 μM DB before adding master mix (50 mM Tris (pH 7.5), 62 μM DCPIP, 20 mM K-succinate (pH 7.5)) immediately prior to measurements. DCPIP reduction was monitored over the initial 30 s linear range. SDH activity is represented as total % change in DCPIP absorbance as compared with 0 mM Ca^{2+}. SQR activity is represented as % change (compared with 0 mM Ca^{2+} addition) in DCPIP absorbance over the initial 30 s time period divided by the initial absorbance.

Mitochondrial immunofluorescence. HeLa cells were seeded on rounded microscope slides placed in a 6-well tissue culture plate at ~125 000 cells per well 24 h prior to transfection. Cells were transfected using the commercial jetPEi protocol with pcDNA3 empty vector or a plasmid encoding cardiolipin synthase-1 (CLS1). Forty-eight hours post transfection, the cells were stained for cardiolipin (CL) expression using CL primary antibody from ImmunoVision and secondary Alexa Fluor 488 Goat Anti-Human IgG antibody from Life Technologies (Paisley, UK). The cells were imaged using the Leica TCS SP5 Confocal.

Calcein AM-based transition pore assay. HeLa cells were harvested following treatment and resuspended in 1 ml of Hanks' Balance Salt Solution with calcium (Gibco, Life Technologies, Paisley, UK), then stained with 2 μM calcein AM along with 0.4 mM cobalt chloride (CoCl2), to quench the staining for mitochondria only, for 15 min at 37 °C in the incubator. Following incubation, the samples were washed using 3.5 ml of Hanks' Balance Salt Solution with calcium, pelleted, and resuspended in 150 μl of PBS. Sample data were acquired using flow cytometer (BD Biosciences) and analyzed with the FlowJo programme (TreeStar Inc.).

Mitochondrial calcium quantification assay. HeLa cells were seeded at approximately 5 500 cells per well in a 96-well black, glass-bottom imaging plate and incubated overnight at 37 °C to allow for recovery. The Leica TCS SP5 Confocal was used to quantify calcium in the mitochondria following a published imaging protocol.[49]

Statistical analysis. Statistical analysis was performed using the unpaired student's *t*-test. In experiments involving transient transfections data presenting induction and inhibition effects were normalized. For this, GFP transfection was performed and the transfection efficiency analyzed in parallel. Three independent experiments ($n = 3$) were used for all FRET, cell death, and ROS assays. Error bars are S.D. SDS-PAGE gels are representative of at least three independent experiments. All activity assay results are presented as means ± S.E.M. of at least four independent experiments. A two-tailed student *t*-test (equal variance) was used to determine statistical significance ($P \leq 0.05$).

Conflict of Interest

The authors declare no conflict of interest.

Acknowledgements. M-S H was supported by a stipend from AstraZeneca R&D, EP by Cancer Research UK, and CD by a fellowship from Breast Cancer Campaign. The Alder lab was supported by a National Science Foundation Grant MCB-1024908 (to NA) and by a National Science Foundation GRFP award (to CS).

1. Orrenius S, Zhivotovsky B, Nicotera P. Regulation of cell death: the calcium-apoptosis link. *Nat Rev Mol Cell Biol* 2003; **4**: 552–565.
2. De Stefani D, Raffaello A, Teardo E, Szabo I, Rizzuto R. A forty-kilodalton protein of the inner membrane is the mitochondrial calcium uniporter. *Nature* 2011; **476**: 336–340.
3. Baughman JM, Perocchi F, Girgis HS, Plovanich M, Belcher-Timme CA, Sancak Y *et al.* Integrative genomics identifies MCU as an essential component of the mitochondrial calcium uniporter. *Nature* 2011; **476**: 341–345.
4. Rizzuto R, Pinton P, Carrington W, Fay FS, Fogarty KE, Lifshitz LM *et al.* Close contacts with the endoplasmic reticulum as determinants of mitochondrial Ca2+ responses. *Science* 1998; **280**: 1763–1766.
5. Albayrak T, Scherhammer V, Schoenfeld N, Braziulis E, Mund T, Bauer MK *et al.* The tumor suppressor cybl, a component of the respiratory chain, mediates apoptosis induction. *Mol Biol Cell* 2003; **14**: 3082–3096.
6. Ishii T, Miyazawa M, Onouchi H, Yasuda K, Hartman PS, Ishii N. Model animals for the study of oxidative stress from complex II. *Biochim Biophys Acta* 2013; **1827**: 588–597.
7. Lenaz G. Mitochondria and reactive oxygen species. Which role in physiology and pathology? *Adv Exp Med Biol* 2012; **942**: 93–136.
8. Cecchini G. Function and structure of complex II of the respiratory chain. *Annu Rev Biochem* 2003; **72**: 77–109.
9. Lemarie A, Huc L, Pazarentzos E, Mahul-Mellier AL, Grimm S. Specific disintegration of complex II succinate: ubiquinone oxidoreductase links pH changes to oxidative stress for apoptosis induction. *Cell Death Differ* 2011; **18**: 338–349.
10. Lutter M, Fang M, Luo X, Nishijima M, Xie X, Wang X. Cardiolipin provides specificity for targeting of tBid to mitochondria. *Nat Cell Biol* 2000; **2**: 754–761.
11. Kuwana T, Mackey MR, Perkins G, Ellisman MH, Latterich M, Schneiter R *et al.* Bid, Bax, and lipids cooperate to form supramolecular openings in the outer mitochondrial membrane. *Cell* 2002; **111**: 331–342.
12. Kagan VE, Tyurin VA, Jiang J, Tyurina YY, Ritov VB, Amoscato AA *et al.* Cytochrome c acts as a cardiolipin oxygenase required for release of proapoptotic factors. *Nat Chem Biol* 2005; **1**: 223–232.
13. Keinan N, Pahima H, Ben-Hail D, Shoshan-Barmatz V. The role of calcium in VDAC1 oligomerization and mitochondria-mediated apoptosis. *Biochim Biophys Acta* 2013; **1833**: 1745–1754.
14. Dibrov E, Fu S, Lemire BD. The Saccharomyces cerevisiae TCM62 gene encodes a chaperone necessary for the assembly of the mitochondrial succinate dehydrogenase (complex II). *J Biol Chem* 1998; **273**: 32042–32048.
15. Crompton M. The mitochondrial permeability transition pore and its role in cell death. *Biochem J* 1999; **341**(Pt 2): 233–249.
16. Li Y, Johnson N, Capano M, Edwards M, Crompton M. Cyclophilin-D promotes the mitochondrial permeability transition but has opposite effects on apoptosis and necrosis. *Biochem J* 2004; **383**(Pt 1): 101–109.
17. Lin DT, Lechleiter JD. Mitochondrial targeted cyclophilin d protects cells from cell death by peptidyl prolyl isomerization. *J Biol Chem* 2002; **277**: 31134–31141.
18. Schubert A, Grimm S. Cyclophilin D, a Component of the Permeability Transition (PT)-Pore, Is an Apoptosis Repressor. *Cancer Res* 2004; **64**: 85–93.
19. Baines CP, Kaiser RA, Purcell NH, Blair NS, Osinska H, Hambleton MA *et al.* Loss of cyclophilin D reveals a critical role for mitochondrial permeability transition in cell death. *Nature* 2005; **434**: 658–662.
20. Nakagawa T, Shimizu S, Watanabe T, Yamaguchi O, Otsu K, Yamagata H *et al.* Cyclophilin D-dependent mitochondrial permeability transition regulates some necrotic but not apoptotic cell death. *Nature* 2005; **434**: 652–658.
21. Schwall CT, Greenwood VL, Alder NN. The stability and activity of respiratory Complex II is cardiolipin-dependent. *Biochim Biophys Acta* 2012; **1817**: 1588–1596.
22. Killian JA, Koorengevel MC, Bouwstra JA, Gooris G, Dowhan W, de Kruijff B. Effect of divalent cations on lipid organization of cardiolipin isolated from Escherichia coli strain AH930. *Biochim Biophys Acta* 1994; **1189**: 225–232.
23. Powell GL, Knowles PF, Marsh D. Spin-label studies on the specificity of interaction of cardiolipin with beef heart cytochrome oxidase. *Biochemistry* 1987; **26**: 8138–8145.
24. Bygrave FL, Benedetti A. What is the concentration of calcium ions in the endoplasmic reticulum? *Cell calcium* 1996; **19**: 547–551.
25. Giorgi C, De Stefani D, Bononi A, Rizzuto R, Pinton P. Structural and functional link between the mitochondrial network and the endoplasmic reticulum. *Int J Biochem Cell Biol* 2009; **41**: 1817–1827.
26. Brenza JM, Neagle CE, Sokolove PM. Interaction of Ca2+ with cardiolipin-containing liposomes and its inhibition by adriamycin. *Biochem Pharmacol* 1985; **34**: 4291–4298.
27. Grijalba MT, Vercesi AE, Schreier S. Ca2+-induced increased lipid packing and domain formation in submitochondrial particles. A possible early step in the mechanism of Ca2+-stimulated generation of reactive oxygen species by the respiratory chain. *Biochemistry* 1999; **38**: 13279–13287.
28. Crimi M, Esposti MD. Apoptosis-induced changes in mitochondrial lipids. *Biochim Biophys Acta* 2011; **1813**: 551–557.
29. Choi SY, Gonzalvez F, Jenkins GM, Slomianny C, Chretien D, Arnoult D *et al.* Cardiolipin deficiency releases cytochrome c from the inner mitochondrial membrane and accelerates stimuli-elicited apoptosis. *Cell Death Differ* 2007; **14**: 597–606.
30. Huang Z, Jiang J, Tyurin VA, Zhao Q, Mnuskin A, Ren J *et al.* Cardiolipin deficiency leads to decreased cardiolipin peroxidation and increased resistance of cells to apoptosis. *Free Radic Biol Med* 2008; **44**: 1935–1944.
31. Gonzalvez F, Schug ZT, Houtkooper RH, MacKenzie ED, Brooks DG, Wanders RJ *et al.* Cardiolipin provides an essential activating platform for caspase-8 on mitochondria. *J Cell Biol* 2008; **183**: 681–696.
32. Shen ZY, Shen WY, Chen MH, Shen J, Cai WJ, Zeng Y. Mitochondria, calcium and nitric oxide in the apoptotic pathway of esophageal carcinoma cells induced by As2O3. *Int J Mol Med* 2002; **9**: 385–390.
33. Tang CH, Chiu YC, Huang CF, Chen YW, Chen PC. Arsenic induces cell apoptosis in cultured osteoblasts through endoplasmic reticulum stress. *Toxicol Appl Pharmacol* 2009; **241**: 173–181.
34. Lemasters JJ, Theruvath TP, Zhong Z, Nieminen AL. Mitochondrial calcium and the permeability transition in cell death. *Biochim Biophys Acta* 2009; **1787**: 1395–1401.
35. Peng TI, Jou MJ. Oxidative stress caused by mitochondrial calcium overload. *Ann N Y Acad Sci* 2010; **1201**: 183–188.
36. Giacomello M, Drago I, Pizzo P, Pozzan T. Mitochondrial Ca2+ as a key regulator of cell life and death. *Cell Death Differ* 2007; **14**: 1267–1274.
37. Ricci JE, Waterhouse N, Green DR. Mitochondrial functions during cell death, a complex (I-V) dilemma. *Cell Death Differ* 2003; **10**: 488–492.
38. Scorrano L, Oakes SA, Opferman JT, Cheng EH, Sorcinelli MD, Pozzan T *et al.* BAX and BAK regulation of endoplasmic reticulum Ca2+: a control point for apoptosis. *Science* 2003; **300**: 135–139.
39. Nutt LK, Gogvadze V, Uthaisang W, Mirnikjoo B, McConkey DJ, Orrenius S. Indirect effects of Bax and Bak initiate the mitochondrial alterations that lead to cytochrome c release during arsenic trioxide-induced apoptosis. *Cancer Biol Ther* 2005; **4**: 459–467.
40. Schoenfeld N, Bauer MK, Grimm S. The metastasis suppressor gene C33/CD82/KAI1 induces apoptosis through reactive oxygen intermediates. *Faseb J* 2004; **18**: 158–160.
41. Lemarie A, Grimm S. Mutations in the heme b-binding residue of SDHC inhibit assembly of respiratory chain complex II in mammalian cells. *Mitochondrion* 2009; **9**: 254–260.
42. Pfeiffer K, Gohil V, Stuart RA, Hunte C, Brandt U, Greenberg ML *et al.* Cardiolipin stabilizes respiratory chain supercomplexes. *J Biol Chem* 2003; **278**: 52873–52880.
43. Yan Y, Marriott G. Analysis of protein interactions using fluorescence technologies. *Curr Opin Chem Biol* 2003; **7**: 635–640.
44. Daum G, Gasser SM, Schatz G. Import of proteins into mitochondria: energy-dependent, two-step processing of the intermembrane space enzyme cytochrome b2 isolated yeast mitochondria. *J Biol Chem* 1982; **257**: 13075–13080.
45. Ranaghan MJ, Schwall CT, Alder NN, Birge RR. Green Proteorhodopsin Reconstituted into Nanoscale Phospholipid Bilayers (Nanodiscs) as Photoactive Monomers. *J Am Chem Soc* 2011; **133**: 18318–18327.
46. Ritchie TK, Grinkova YV, Bayburt TH, Denisov IG, Zolnerciks JK, Atkins WM *et al.* Reconstitution of Membrane Proteins in Phospholipid Bilayer Nanodiscs. *Met Enzymol* 2009; **464**: 211–231.
47. Hao HX, Khalimonchuk O, Schraders M, Dephoure N, Bayley JP, Kunst H *et al.* SDH5, a gene required for flavination of succinate dehydrogenase, is mutated in paraganglioma. *Science* 2009; **325**: 1139–1142.
48. Lemaire C, Dujardin G. Preparation of respiratory chain complexes from Saccharomyces cerevisiae wild-type and mutant mitocondria. *Met Mol Biol* 2008; **432**: 65–81.
49. Davidson SM, Duchen MR. Imaging mitochondrial calcium signalling with fluorescent probes and single or two photon confocal microscopy. *Met Mol Biol* 2012; **810**: 219–234.

Supplementary Information accompanies this paper on Cell Death and Differentiation website (http://www.nature.com/cdd)